High-flux normal incidence monochromator for circularly polarized synchrotron radiation

F. Schäfers and W. Peatman

Berliner Elektronenspeicherring Gesellschaft für Synchrotronstrahlung mbH, Lentzeallee 100, D-1000 Berlin 33, West Germany

A. Eyers, Ch. Heckenkamp, G. Schönhense, and U. Heinzmann

Fritz-Haber-Institut der Max-Planck-Gesellschaft, Faradayweg 4-6, D-1000 Berlin 33, West Germany and Fakultät für Physik der Universität Bielefeld, D-4800 Bielefeld, West Germany

A 6.5-m normal incidence monochromator installed at the storage ring BESSY, which is optimized for a high throughput of circularly polarized off-plane radiation at moderate resolution is described. The monochromator employs two exit slits and is specially designed and used for low-signal experiments such as spin- and angle-resolved photoelectron spectroscopy on solids, adsorbates, free atoms, and molecules. The Monk–Gillieson mounting (plane grating in a convergent light beam) allows for large apertures with relatively little astigmatism. With two gratings, a flux of more than 10^{11} photons s^{-1} bandwidth^{-1} (0.2–0.5 nm) with a circular polarization of more than 90% in the wavelength range from 35 to 675 nm is achieved.

INTRODUCTION

The increasing demand for a high flux of radiation in the VUV and soft x-ray region has led to the development of storage rings dedicated and optimized for the production of synchrotron radiation. With these second generation devices, special emphasis can be put on the optimal matching of the beam line optics to the characteristics of the radiation and the light source with respect to the source dimensions and the brightness of the radiation. With the development of monochromators by which special requirements for throughput, bandpass, second-order rejection, and/or polarization can be met, experiments of hitherto unachievable sophistication have become possible. The number of books,[1-3] conference proceedings,[4-6] and review articles contained in the proceedings dealing with synchrotron radiation, its instrumentation, and its applications demonstrates the increasing importance of this rapidly developing area in basic research.

This paper describes a monochromator at the Berlin Electron Storage Ring (BESSY), which exploits the circular polarization of the light emitted from the ring and is optimized to yield a high flux of dispersed radiation. It has been specially designed for low-signal experiments such as spin- and angle-resolved photoelectron spectroscopy of atoms, molecules, solids, and adsorbates. The only device which has previously been reported to deliver circularly polarized VUV-synchrotron radiation is the 10-m normal incidence monochromator at the Bonn Synchrotron[7,8] yielding a flux of 10^9 photons s^{-1}. The aim of the new design, which has been described briefly earlier,[9] was to combine the high circular polarization with intensities that are usually obtained at other experimental stations for photoemission or luminescence studies, where fluxes of 10^{11}–10^{12} photons s^{-1} nm^{-1} of partially linearly polarized light have been reported.[10-13]

The monochromator has two exit slits which can be supplied alternatively with light, thus enabling two experiments to be set up simultaneously. It uses the radiation which is emitted above and below the plane of the storage ring (off-plane) at a beam port delivering radiation of 50 mrad horizontal and 10 mrad vertical divergence. The two components of the synchrotron radiation polarized perpendicularly to each other are superimposed with a phase difference of 90° thus yielding elliptically polarized light.[14-16] The component polarized perpendicularly to the orbit plane vanishes in the plane. Therefore, the in-plane radiation is linearly polarized, while the off-plane radiation has a high degree of circular polarization.[7]

The large acceptance and the demand for a high degree of polarization made a normal incidence mounting necessary to keep aberrations and depolarization small, thus limiting the energy range to $hv < 35$ eV. The demand for the highest throughput of circularly polarized light implied that no entrance slit should be used, entrance and exit arms should be as large as possible to increase the resolution, a horizontal dispersion plane be used to favor the reflection of the component polarized perpendicularly to the orbit plane, and not more than two reflections should be used.

Due to these restrictions the conventional Seya–Namioka and the Rowland circle mounts were rejected, since these types cannot be used with such large apertures or only with suitable prefocusing optics.[17-20] In addition, the Seya–Namioka has large astigmatism and significantly modifies the polarization of the incident radiation.

The criteria stated favored the decision to design a Monk–Gillieson-type monochromator which up to now has not been used with synchrotron radiation. The basic principle of this mounting, which is schematically shown in Fig. 1, is the use of a plane grating in a convergent light beam, hence, the dispersing and focusing are realized by two different elements.

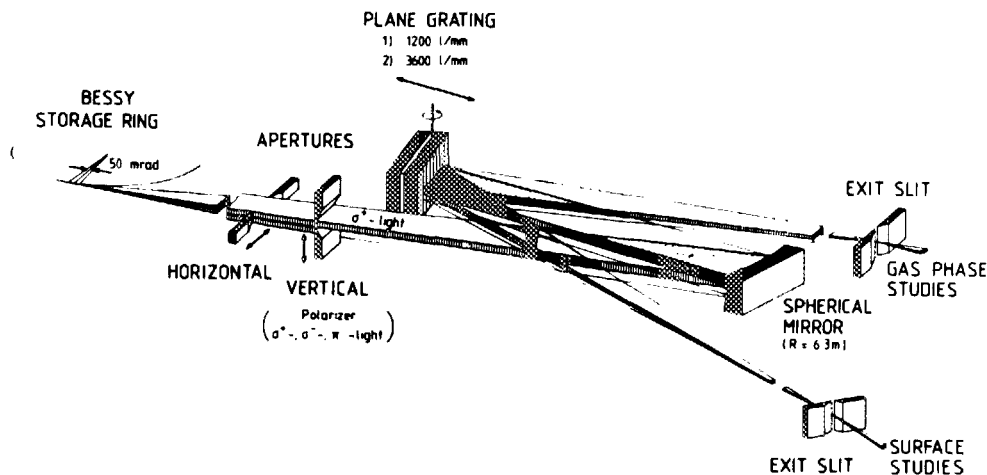The spherical mirror produces an image of the electron

FIG. 1. Optical configuration of the 6.5-m normal incidence monochromator at BESSY.

beam (virtual entrance slit) and the plane grating disperses the light horizontally onto one of two exit slits mounted symmetrically with respect to the incident light in positive and negative first order. The exit slits are integrated into the experimental chambers where gas phase studies (separated by a differential pumping stage) and surface studies, respectively, are to be performed. The degree of circular polarization of the light can be varied by the use of two vertical apertures in front of the monochromator which select the radiation emitted above or below the orbit plane (σ^+ and σ^- light, respectively). Horizontal apertures may be used to reduce the aberrations, when an increased resolution is desired.

The theory of this mounting was developed by Monk.[21] Twenty years later, Gillieson,[22] and later Hall,[23] reformulated and extended the theoretical treatment and showed that the astigmatism can be made zero at one wavelength and that the dispersion is more uniform than that of the Wadsworth mounting. Schröder[24] developed design principles for the optimization by which the third-order aberrations for coma and astigmatism can be compensated for at one wavelength by a proper choice of the grating and premirror parameters. He also discusses the problem of compensating for the defocusing by an eccentric rotation of the grating.[25] Murty[26] and Smyth[27] discuss the possibility of producing stigmatic images by various types of mountings and prefocusing mirrors. In addition, other authors have developed ray tracing methods for the plane grating monochromator.[28,29]

The most striking advantages of this mounting are the possibility of using large apertures with long arm lengths to enhance the obtainable resolution and the use of only one nonplanar surface to keep the costs in limit. This element, a spherical mirror, can be made to a high figure and at a payable price despite the large dimensions. The use of a plane grating as the only other optical element has the advantage that such gratings can be obtained in the required size and ruling densities with the further advantage of greater efficiency as compared with concave gratings. The instrument has low astigmatism compared with Rowland circle mountings.

After a brief summary of the theory (Sec. I), the optical and technical layout and the design principles of the BESSY

version of the Monk–Gillieson mount are presented in Sec. II. In Sec. III results of the optical measurements (resolution, intensity, polarization) are shown. Some examples of the experimental activities connected with this monochromator concerned with spin- and angle-resolved photoelectron spectroscopy at atoms, solids, and adsorbates are presented in Sec. IV.

I. THEORY

The theory of the Monk–Gillieson monochromator has been extensively treated by Monk,[21] Gillieson,[22] and others.[23-29] Therefore only the main results will be summarized here and outlined along the lines of Fig. 2, where the general optical layout and the nomenclature used is shown. Only the principle ray is plotted for both positive and negative order of diffraction, following the definition of Samson.[30]

The spherical mirror (radius R) deflects the incoming light beam (entrance arm length r) by the angle 2ϕ and produces a virtual image behind the grating. Due to the astigmatism of the mirror, the vertical focus lies behind the horizontal focus (exit arm lengths r_v and r_h, respectively). The separation of the two foci can be calculated according to
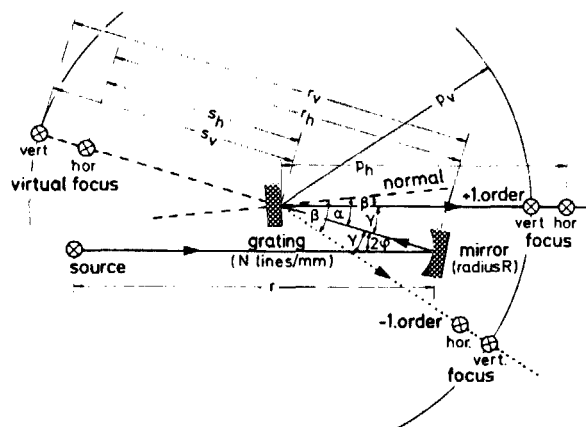

FIG. 2. Geometry of the Monk–Gillieson mounting.

Beutler[31] and Namioka[32]

$$\frac{\cos^2 \alpha}{r} - \frac{\cos \alpha}{R} + \frac{\cos^2 \beta}{r_h} - \frac{\cos \beta}{R} = 0 \qquad (1)$$

and

$$\frac{1}{r} - \frac{\cos \alpha}{R} + \frac{1}{r_v} - \frac{\cos \beta}{R} = 0 \qquad (2)$$

and letting $\alpha = \beta$.

The astigmatism is given by

$$Z/L_M = (2r_v/R) \sin \phi \tan \phi , \qquad (3)$$

where L_M is the height of the mirror.

The tangential coma of the mirror, which determines the separation between the intersection of the marginal rays and the chief ray in the horizontal direction is

$$C_M = 3(1 - M) y^2 \phi /2R , \qquad (4)$$

where y is the horizontal semiaperture of the mirror.

The sign and the direction of the coma flare depends on the magnification of the mirror $M = r_h/r$ ($C_M > 0$: coma flare away from the mirror axis). By putting a plane grating into the convergent light beam between the mirror and the virtual focus at an angle α with respect to the grating normal, the beam is vertically reflected and horizontally a dispersion plane is established. In this plane the vertical foci lie on a circle with radius s_v ($= p_v$) around the grating center.

The ray-tracing calculations start as usual with the introduction of the light path function F and, in order that a focal point is to be produced, letting F be an extremum at this point according to Fermat's principle ($\partial F / \partial r = 0$). The series expansion of this expression yields the grating equation in the first-order approximation. The higher orders determine the focus curve and the aberrations, the main ones being coma and astigmatism.[23]

The mounting satisfies the general grating equation

$$m\lambda = d(\sin \alpha + \sin \beta) = d \left[\sin \alpha + \sin(\alpha - \gamma) \right] , \qquad (5)$$

where d is the grating constant ($1/N$, $N =$ lines/mm) and m the order of diffraction.

The focal point equation is

$$p_h = s_h (\cos^2 \beta /\cos^2 \alpha) = s_h \cos^2 \gamma (1 + \tan \gamma \tan \alpha)^2 . \qquad (6)$$

Thus the focus curve has no constant radius of curvature and for a fixed angle of incidence α, Eq. (6) is the equation of a lemniscate ($p_h = \text{const} \cos^2 \beta$).[21] The linear dispersion is given by

$$\frac{dl}{d\lambda} = \frac{ms_h \cos \beta (1 + 4 \tan^2 \beta)^{1/2}}{d \cos^2 \alpha} . \qquad (7)$$

Except for the factor $(1 + 4 \tan^2 \beta)^{1/2}$, which is close to unity at small angles, the dispersion closely resembles that of the Rowland circle mount and is almost linear.

The third-order aberrations produced by the plane grating can be calculated according to

1. Astigmatism

$$\frac{Z'}{L_g} = \frac{\cos^2 \beta}{\cos^2 \alpha} - 1 , \qquad (8)$$

L_g corresponds to the illuminated length of the grating rulings.

2. Coma

$$C_g = \frac{3}{2} \frac{l^2 Nm\lambda}{s_h} , \qquad (9)$$

l is the horizontal semiaperture of the grating. C_g is positive when the coma flare is away from the grating normal.

The contributions to astigmatism and to coma from both the grating and the mirror can be made zero for wavelengths which are determined by a proper choice of the design parameters.[23,25]

To use this instrument as a scanning spectrometer it is essential that the exit slit, located at the horizontal focus, be fixed. It is seen from Eq. (6), however, that the distance p_h from the grating to the exit slit is a function of α and hence the wavelength. This effect must be compensated for by a translation of the grating. The fraction p_h/s_h equals 1 at the zero-order position and at the positive order of diffraction (focus 1) it increases as α increases. Therefore, the grating must be displaced from the exit slit with increasing wavelength. The situation in the negative order (focus 2), however, is reversed since here p_h/s_h decreases in going to longer wavelengths and the grating must be moved towards the exit slit.

II. DESIGN PRINCIPLES

A. Optical layout

The monochromator was layed out for the beamline 32.10 of the BESSY storage ring[33,34] supplying radiation of 50 mrad horizontal and 10 mrad vertical divergence. The front end and radiation wall take up the first 3.5 m from the tangent point of the ring. In order to achieve a normal incidence reflection of the incoming light in the horizontal plane without interfering with the neighboring beam line the focusing mirror was set at a distance of 6.5 m from the source with a deviation angle of $2\phi = 8°$ and producing a 1:1 image.

The mean distance between mirror and grating was set at 2 m and the requirement of two exit slits suggested a symmetrical mount using both the positive and negative first-order radiation, at a deviation angle between the incoming and outgoing light beams of $\gamma = + 8°$ and $- 8°$, respectively. Therefore, the diffracted beam in positive order (exit 1) is parallel to the beam from the storage ring with a horizontal displacement of 278 mm, while the negative-order beam emerges with an angle of 16° to the incident beam from the ring. This layout provides an adequate clearance between the optical elements and the light bundles and between the two foci, which are to be integrated into two different experimental chambers.

Once γ has been fixed for a fixed mirror-grating distance ($= \gamma_0$), the angles of incidence and diffraction, α and β, can be calculated according to Eq. (5), using a suitable grating constant and wavelength. Then the exit arm lengths (p_0) can be determined using Eq. (6).

For a wavelength scan the grating has to be rotated and translated in the direction of the incoming light beam. After some geometrical considerations the equations for the displacement of the grating (with respect to the middle posi-

tion) determined by p_0, s_0, and γ_0 read

$$p_h = p_0 \sin \gamma_0 / \sin \gamma \qquad (10)$$

and

$$s_h = s_0 + p_0 \cos \gamma_0 - p_h \cos \gamma . \qquad (11)$$

From Eq. (6) follows:

$$\tan \alpha = (p_h / s_h)^{1/2} - \cos \gamma / \tan \gamma . \qquad (12)$$

γ is chosen as an arbitrary parameter.

The wavelength range that should be covered by two gratings of 1200 and 3600 1/mm is from zero order to 675 and 225 nm, respectively. In this range γ varies by 5%. The translation of the grating corresponding to these wavelength ranges totals 300 mm and is linear with the wavelength within 3%.

Starting with Eqs. (10)–(12) the linear dispersion and the aberration terms can be calculated from Eqs. (7)–(9). The results are shown in Fig. 3.

In the upper part [Fig. 3(a)] the linear dispersion $d\lambda/dl$ is shown for both gratings in both positive and negative order. The dispersion is slightly different for both orders with a crossover point, the difference between the two gratings being the scaling factor $N_{grating\ 1}/N_{grating\ 2}$.

The astigmatism and coma are shown in Fig. 3(b). The ordinate at the right side determines the distance between the horizontal and vertical focus. It is seen that the astigmatism (full line) nearly increases linearly with wavelength. At zero order, the astigmatism is due to the spherical mirror only. In positive order the image is stigmatic at 80 nm, since the astigmatism of mirror and grating compensate for each other. The tangential coma (dashed line) of the grating increases linearly with wavelength. Compared with the grating coma the coma of the mirror (zero order) can be neglected. The coma flares of both orders are directed towards the mirror.

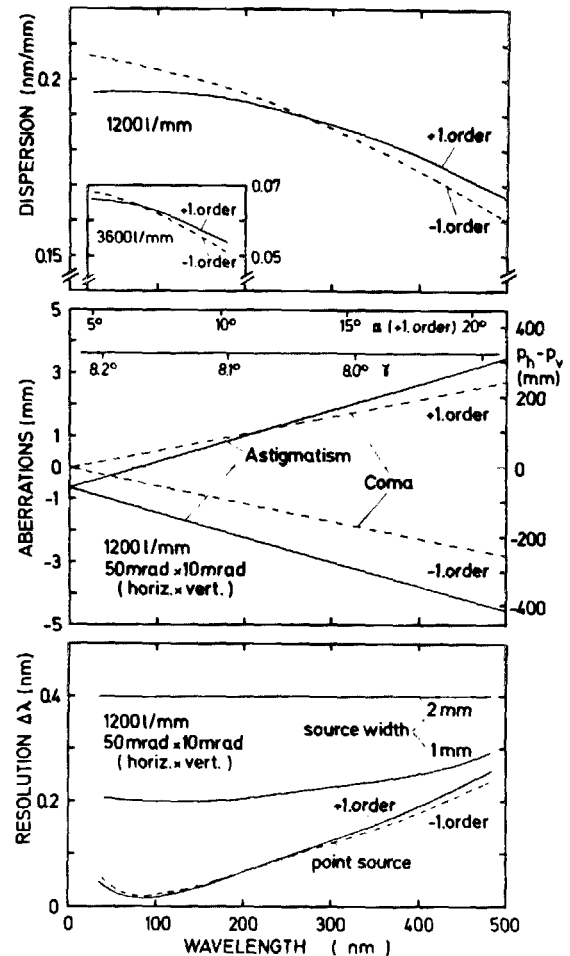An evaluation of ray-tracing calculations performed

FIG. 3. Optical performance of the monochromator. (a) linear dispersion $d\lambda/dl$ of both gratings in both positive and negative first order. (b) main aberrations of the design: astigmatism and tangential coma. The ordinate at the right side is the distance between the horizontal and the vertical focus. (c) resolution $\Delta\lambda$, according to ray tracing calculations for a point source, 1- and 2-mm entrance slit, respectively.

TABLE I. Details of the system.

	Mirror	1st grating	2nd grating
surface	spherical	plane	plane
material	Aluminum + Kanigen	quartz	spectrosil
coating	Os	Al + MgF$_2$	Os
groove density (1/mm)	—	1200	3600
wavelength range (nm)	—	0–675	0–225
groove profile	—	sinusoidal	
radius (mm)	6309	—	
dimensions (mm^3)	365 × 80 × 65	260 × 140 × 60	
distance from entrance slit (r) (mm)	6500	—	
distance to mirror ($r_h - s_h$) (mm)	—	2000 ± 150	
distance to exit slit 1 (p_h) (mm)	—	4320 ± 150	
distance to exit slit 2 (p_h) (mm)	—	3858 ± 150	
deviation angle 2 $\phi(\gamma)$	8°	8° ± 0.2°	

confirms these results [Fig. 3(c), lower part]. Assuming a point source the aberration limited resolution is optimized in the region of 80 nm and worsens with increasing wavelength due to the larger angles of incidence. Taking a source size of 1 and 2 mm horizontally (upper curves), respectively, has the effect of smoothing out the wavelength dependence of the resolution, so that in the VUV region a practically constant source size limited resolution is obtained. Thus the resolution is proportional to the horizontal dimension of the stored electron beam.

Table I summarizes the main parameters of the monochromator.

B. Technical layout

The technical design of the monochromator was developed in cooperation with Bird & Tole Ltd. and Chelsea Instruments Ltd., England. One large vacuum vessel for both mirror and grating is employed, necessitated by the large acceptance (illuminated area of the mirror: 325×65 mm^2), the small deviation angles, and the clearance for the optical path. The main technical features are sketched schematically in Fig. 4.

The monochromator tank with a volume of approximately 2 m^3 is built to ultra high-vacuum standards (UHV), and consists of three cylindrical tubes of 800–900 mm diameter which are connected by goldwire seals, the domed end sections containing the entrance and the two exit flanges. It is equipped with two 400-1/s ion pumps maintaining a vacuum of 1×10^{-9} mbar after bakeout at 80 °C with all optical components installed. During operation the temperature of the entire tank is thermostatically stabilized slightly above room temperature. Mirror and grating are mounted on an optical bench (dashed area) which is fixed to the middle tube. The optics can, therefore, be prealigned with the end tubes removed and are unaffected by their installation and by evacuation of the tank.

The mirror is mounted on one end of the optical bench. It is tippable from outside to keep the focal point fixed if the beam position in the storage ring should change. Water cooling is provided to dissipate the high heat loading of approximately 80 W at a typical 500-mA BESSY current. The thermal stress of the mirror is, however, relaxed somewhat because the vertical apertures in front of the monochroma-
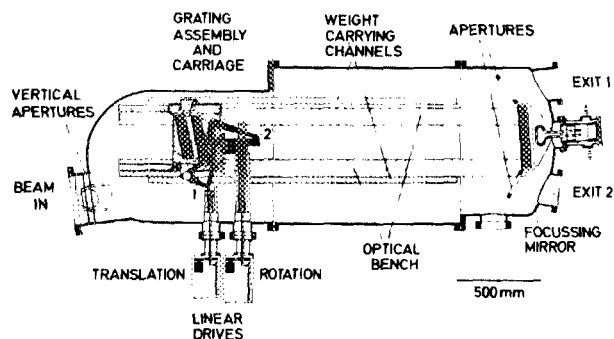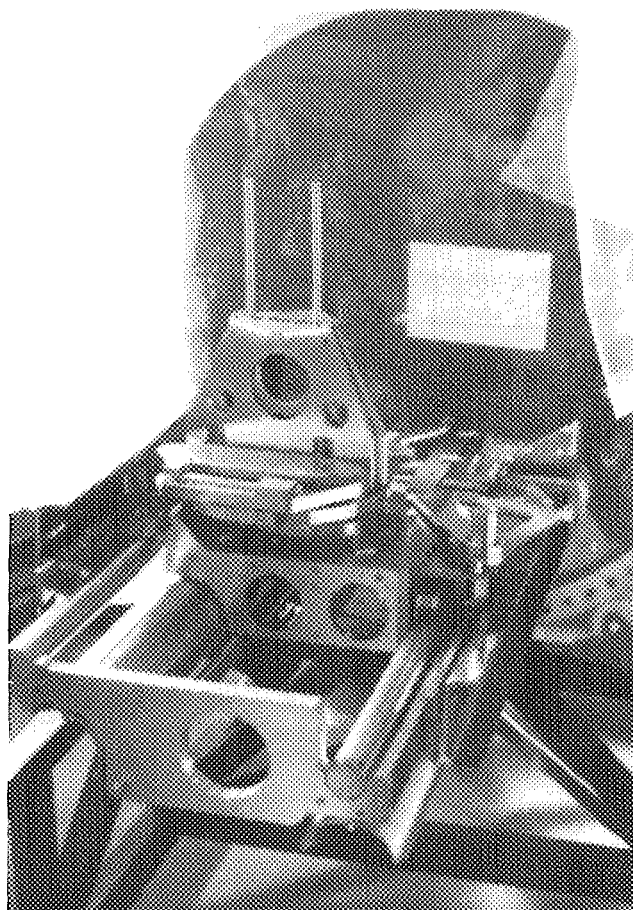

FIG. 5. View of the grating assembly (seen from the storage ring). Part of the optical bench and the weight carrying channels can be seen.

tor normally cut out the x-ray component of the synchrotron radiation emitted in the orbit plane, since only the off-plane radiation is used with this monochromator.

The grating assembly (Fig. 4 dotted area) is shown in detail in Figs. 5 and 6. In Fig. 5, the view is from the storage

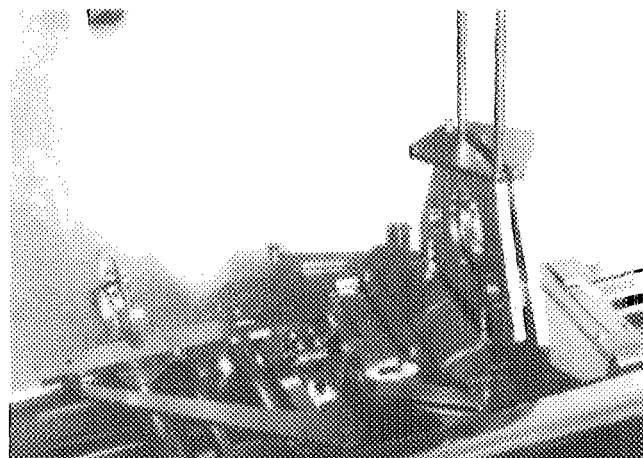FIG. 4. Technical performance of the monochromator.

FIG. 6. View of the grating holders and the translation and rotation mechanism. The incident light comes from the left side.

ring [the mirror is in the back (not shown)] and part of the optical bench and of the weight carrying channels together with the grating carriage, grating base, and the grating holders is seen.

In Fig. 6, the light incident on the grating comes from the left. The two adjustable grating holders and part of the translation and rotation mechanism is shown.

The grating base accepts two gratings (black rectangular areas in Fig. 4), each one in a special adjusting assembly. They can be exchanged without breaking vacuum by rotating the common base, which is kinematically mounted on the grating carriage, by 180° around a vertical axis, the end positions being fixed magnetically. The gratings may be positioned at three different heights to illuminate different areas: each grating (260×140 mm^2) consists in effect of three grating strips.

The grating carriage is kinematically mounted and guided along two guide bars (dashed area) which are connected to the optical bench. The carriage has a special suspension by means of which the bulk of the weight is carried by two channels which are attached to the tank, while the precise motion is determined by the optical bench (see Fig. 5).

Since the focus curve is different for each exit arm the rotation and translation of the gratings must be performed independently of each other. This is realized by two linear feedthroughs, each with a stepping motor drive and a precision linear readout with an accuracy of 10 μm $\triangleq$ 3 arcsec/step.

The translation is performed with the left linear feedthrough, whose motion is transferred to the grating assembly by the triangular shaped traverse lever (black area #1) pivoted around one corner. During translation the other lever arm (black area #2) which is fixed to the grating assembly, glides along a polished bar (double dashed area) which is directed along the direction of motion thus not affecting the rotational position. The bar itself is connected to the right-hand feedthrough and can be moved linearly perpendicular to the direction of the grating translation, while the lever arm is always kept in contact with the bar by a retaining spring, thus performing a rotation of the grating.

The stepping motor drives for the translation and rotation of the grating as well as for the two vertical apertures in front of the monochromator are connected to a motor drive unit. The drivers controlling section consists of a Z80 CPU with memory stored in ROM's and an RS 232 link. Positional information for the grating motion is derived from two Heidenhain scales.

The conversion of the input data into a hexadecimal form compatible with the Z80 is performed by an Apple II minicomputer, which itself is connected with an RS 232 link with the BESSY computer system.

The focus curves for each of the gratings are stored in the Apple's memory and are compensated for horizontal dislocations of the electron beam allowing a constant wavelength scan in a variety of speeds, the total range being scannable in 6 min.

The monochromator is separated from the two experiments by two all-metal valves. A pressure difference of 10^4

between the monochromator and the gas phase experiment (exit 1) is maintained by a twofold differential pumping system equipped with a 500- and a 200-1/s turbomolecular pump. The exit slit of 2×6 mm^2 (horizontal $\times$ vertical) is integrated into the experimental chamber and is the opening of the first pumping stage.

The UHV-experimental chamber (exit 2) is coupled directly to the monochromator. A system of apertures define the light path to the exit slit which is integrated into the chamber. For the suppression of higher orders, a LiF-, suprasil-, or quartz-window can be inserted into the light beam.

For adjustment purposes a beam position monitor based on the photoinduced current on a tantal wire that can be scanned vertically through the undispersed radiation in front of the monochromator is used.

The polarization of the radiation can be monitored on line on exit 1 during an experiment with a gold-coated four-mirror analyzer[7,8,35] which is rotatable around the direction of the light. The intensity is measured with an open multiplier with a CuBeO cathode ($\lambda < 120$ nm) or with an absolutely calibrated photodiode (CsSb cathode with LiF window) ($\lambda > 115$ nm).

Since both experiments employ photoelectron spectroscopy this method is routinely used for the wavelength calibration of the monochromator and other performance tests with known substances. This method performed in the VUV region has proved to be more accurate and reliable than using visible He–Ne laser radiation. For this either the energetic position of certain atomic features or of the Fermi edge of solids in spectra obtained with synchrotron radiation may be compared with the corresponding features in spectra generated with HeI resonance line radiation. In addition, the energetic position of atomic autoionization structures, which are very accurately known from absorption measurements, may be used as calibration points.

III. EXPERIMENTAL RESULTS

The experimental possibilities for diagnosis of the monochromator performance comprise: (1) intensity measurements of the undispersed light with a beam position monitor in front of the monochromator, (2) intensity measurements of the dispersed light behind the two exit slits with a multiplier, a calibrated photodiode, or by means of yield measurements on solids, (3) measurements of the linear and circular polarization of the dispersed light, and (4) photoelectron spectroscopy (PES) of atoms, adsorbates, and solids. As free parameters in 1–4 the wavelength and/or the horizontal and vertical apertures may be scanned. The experimental results for the wavelength resolution, the polarization, and the photon flux of the monochromatized radiation obtained with these techniques will be presented in this chapter.

Figure 7 shows the resolution of the monochromator obtained at exit slit 1 with a sodium lamp of 1 mm real entrance slit measured before the monochromator was installed on the ring.[9] Practically no aberrations are present with an acceptance of 12 mrad horizontal (lower curve) and the resolution is in accordance with the dispersion [Fig.
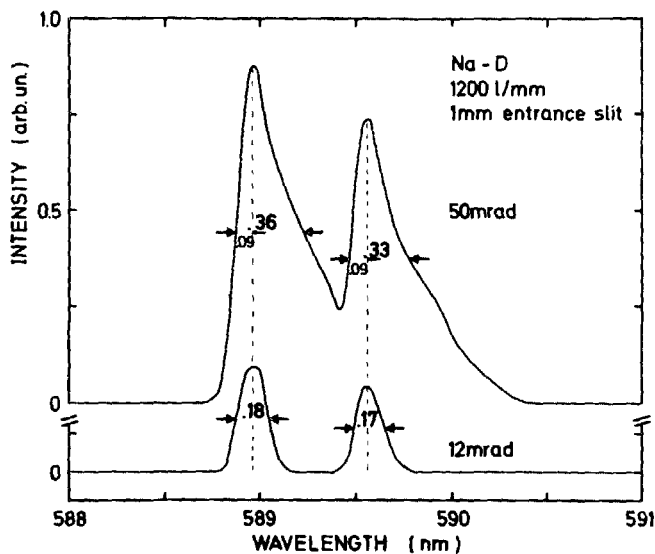
FIG. 7. Resolution obtained with a sodium lamp at two different horizontal acceptances.[9]

3(a)]. The asymmetric aberration broadening due to the coma is clearly seen at 50 mrad acceptance (upper curve). The coma flare is directed towards longer wavelengths, i.e., towards the mirror, as was predicted by theory (Sec. I). The resolution is in good agreement with the ray-tracing calculations [Fig. 3(c)].

The resolution obtained using synchrotron radiation was determined by observing the autoionization resonances between the $5p^5\,{}^2P_{3/2}$ and $5p^5\,{}^2P_{1/2}$ thresholds of atomic Xe by means of photoelectron spectroscopy. A scan of these resonances is shown in Fig. 8 and demonstrates that a spectral bandpass of (0.18 ± 0.05) nm is achieved with the 3600-1/mm grating for a 2-mm exit slit.

Similarly, the resolution of the 1200-1/mm grating was measured by observing the photoelectron peak widths ΔE at different wavelengths from which the spectrometer and the monochromator resolution can be deduced separately according to

$$(\Delta E)^2 = (\Delta E_{\text{sp}})^2 + (\Delta E_{\text{mono}})^2. \qquad (13)$$

A value of $\Delta\lambda = (0.5 \pm 0.05)$ nm was obtained which is, as expected, a factor of 3 larger than the bandpass of the other grating. According to Fig. 3(c) this value corresponds

to an effective source width of about 2.5 mm (FWHM). This width is composed of the actual width of the electron beam and a contribution of 1.2 mm due to the curvature of the orbit along the 50-mrad acceptance, since the source seen by the monochromator extends along the orbit a distance $\theta R/2$ (θ: horizontal acceptance). The width of the electron beam is nearly independent of the stored current according to measurements with another optical system,[36] but is influenced by the machine parameters.

The polarization of the dispersed radiation is essential for the experiments being run on this monochromator: the circular polarization of the off-plane radiation in particular. The components polarized parallel and perpendicular to the storage ring plane and their sum are plotted in Fig. 9 as function of the vertical angle with respect to the orbit plane ($\psi = 0$). The measurements were performed by scanning the vertical apertures in front of the monochromator ($\Delta\psi = 0.25$ mrad) and recording the intensity behind the four-mirror analyzer at two azimuthal angles of $\phi = 0°$ and 90°, respectively. The half-width of the total intensity profile is in full agreement with calculations.

The phase of the two components is shifted by 90° with respect to each other, thus yielding elliptically polarized light (positive ψ: left handed; negative ψ: right handed, according to the optical convention). This has been checked with a quarter-wave plate ($\lambda = 300$ nm) and a Glan prism as linear analyzer.[9] With this setup a total polarization of

$$P = (P_{\text{lin}}^2 + P_{\text{circ}}^2)^{1/2} = 1$$

has been measured. The linear polarization is defined as

$$P_{\text{lin}} = (I_{\parallel} - I_{\perp})/(I_{\parallel} + I_{\perp}). \qquad (14)$$

The circular polarization is for $P = 1$ given by

$$P_{\text{circ}} = \frac{2}{(I_{\parallel}/I_{\perp})^{1/2} + (I_{\perp}/I_{\parallel})^{1/2}}. \qquad (15)$$

Figure 10 shows the linear and circular polarization as function of ψ at a wavelength of 100 nm. The upper curve [Fig. 10(a)] has been measured with a vertical opening of $\Delta\psi = 0.25$ mrad (horizontal error bar), while in Fig. 10(b) the accepted angular range is from ψ to ± 5 mrad.[37] For comparison the results of calculations according to Schwinger's theory[38] are plotted as dashed lines. A quantitative agreement is obtained except for some minor deviations in the orbit plane and far out of the plane. The beam size, which is not included in the calculations, leads experimen-
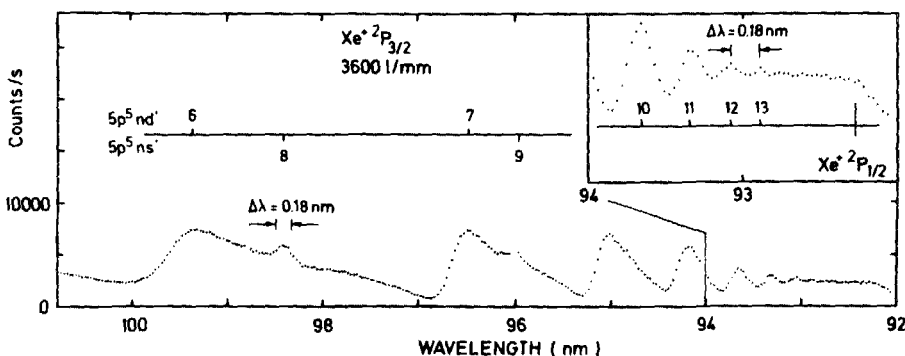

FIG. 8. Autoionization resonances in atomic xenon between the $5p^5\,{}^2P_{3/2}$ and $5p^5\,{}^2P_{1/2}$ limits. The monochromator bandwidth is shown by the vertical bars.
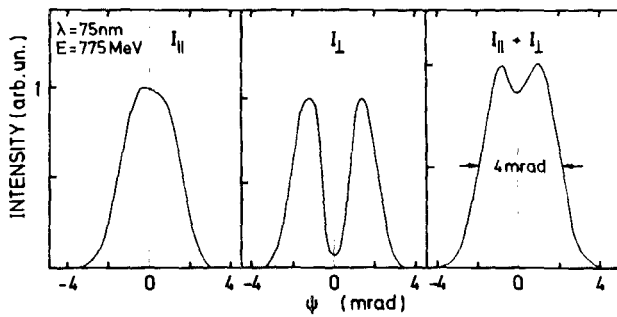
FIG. 9. Relative azimuthal intensity of the components, linearly polarized parallel and perpendicular with respect to the storage ring plane, and their sum measured at 75 nm.

tally to a smearing out of the theoretical values of 100% and 0% for P_{lin} and P_{circ} at $\psi = 0$ in the differential curve. The deviations at large angles may be due to stray light contributions. The measured drop off of the intensity with respect to the total intensity from -5 to $+5$ mrad in going to larger angles is plotted in the lower part as a full line.

Figure 10 demonstrates that depolarization effects of the monochromator are negligibly small. In addition, the differential curve shows that the polarization is an excellent
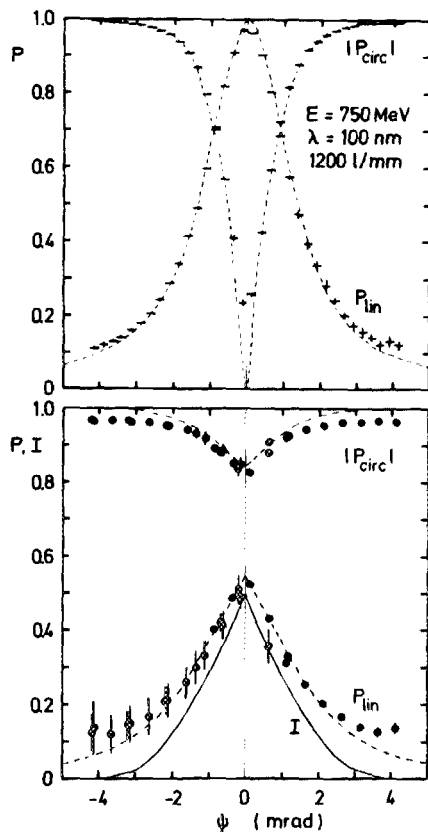
FIG. 10. Azimuthal dependence of the degree of the linear and circular polarization of 100-nm radiation. (a) Differential measurement with a vertical opening of 0.25 mrad (horizontal error bar).[37] (b) integral measurement with a slit from ψ to $\pm$ 5 mrad (error bars).[37] Full curve: ratio of the corresponding measured intensity of the radiation to the total radiation from -5 to $+5$ mrad. The dashed curves indicate the calculated polarization of the incident beam.
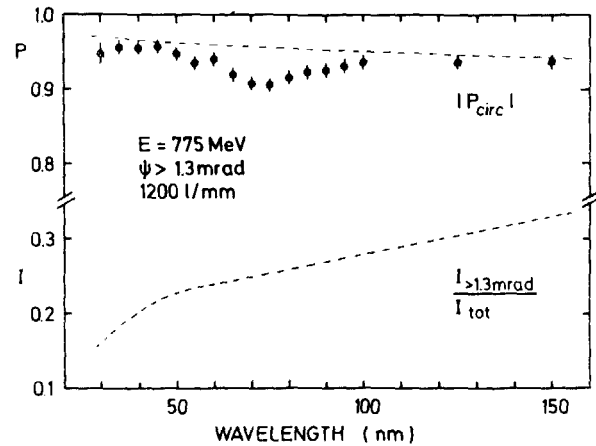
FIG. 11. Wavelength dependence of the circular polarization of the radiation emitted at $\psi > 1.3$ mrad. Error bars: experimental results for the Al–MgF$_2$ grating[39] obtained behind the exit slit 1. Curves: calculated results for the (1) polarization of the incident beam (upper curve), (2) corresponding intensity of the incident radiation as compared with the total intensity from -5 to $+5$ mrad (lower curve).

tool for monitoring the electron beam position. Only the minimum of the circular polarization in the plane has to be determined for the actual orbit plane to be defined. This is performed routinely after each injection.

Figure 11 shows that the polarization measured with the Al–MgF$_2$ grating is nearly independent of the wavelength in the VUV region except for a small dip around 70 nm, which may be due to the optical components.[40] [The Al–MgF$_2$ reflectivity has a minimum in this wavelength range (see Fig. 12).] The upper dashed curve is the calculated polarization of the beam incident on the monochromator premirror. The good agreement between the measured and the calculated values of the polarization indicates that the optics do not modify the photon polarization significantly. Thus, to obtain light with a degree of 92%–95% circular polarization in the VUV region the accepted vertical angular range must be restricted to $\psi > 1.3$ mrad. This causes a reduction of the intensity to 15%–30% (lower dashed line) as compared with the total intensity.
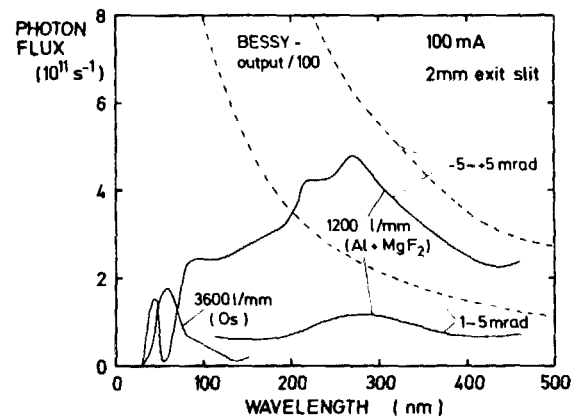
FIG. 12. Absolute photon flux of the dispersed radiation measured behind the exit slits. Full curves: experimental results for two vertical ranges and both gratings at 35 mrad horizontal acceptance. Dashed curves: BESSY output divided by 100.

The purpose of the present design was to deliver the maximum photon flux to the experiments attached to the exit slits. The intensity has therefore been measured with an absolutely calibrated photodiode. The results are shown in Fig. 12 as full lines. The upper curve is valid for full vertical acceptance, the lower one for approximately 90% circularly polarized light. Below the LiF cutoff at 115 nm the photoelectric yield of Pt(111) has been measured and the normalized results have been fitted to the absolute values in the region of overlap. Those results are confirmed by intensity measurements on the other exit slit using an open multiplier which yields the same wavelength dependence. Above 270 nm, the flux follows the shape of the BESSY output (dashed lines, divided by 100), the total transmission of the beam line being approximately 1% maximum. Below 270 nm, the flux is mainly determined by the structured reflectivities of the optical components.

The surprising peaked intensity of the Al–MgF$_2$ 1200-1/mm grating around 45 nm, that has also been observed on other monochromators,[12] may be due to the Al coating while the shoulder at 160 nm arises from the maximum of the osmium reflectance of the mirror.[41] The Al–MgF$_2$ grating is optimized at 120 nm, the Os-coated 3600-1/mm grating around 60 nm, which corresponds to a maximum reflectivity of Os and to a minimum of the other grating efficiency.

The output over the whole wavelength range covered from 35 nm to the visible is more than 2×10^{11} photons s^{-1} bandwidth^{-1} 100 mA^{-1} stored current. At BESSY currents of up to 800 mA the flux exceeds the output of many discharge lamps with the further advantages of tunability and polarization of which every degree from complete circular to linear polarization can be selected.

IV. EXPERIMENTAL ACTIVITIES

Since this monochromator went into operation in the autumn of 1982, the experiments which are connected permanently to the two exit slits are being performed alternatively. The goal of these experiments is the investigation of the electronic structure of atoms, molecules, solids, and adsorbates by means of spin- and angle-resolved photoelectron spectroscopy with circularly polarized radiation. In the gas phase experiment (exit 1),[37] the photoelectron spin polarization of closed shell atoms such as Xe and Hg has been investigated. The spin polarization analysis is connected with an intensity loss of 10^3 due to the efficiency of the spin analyzer (Mott detector). Therefore, for reasonable statistics an accumulation time of up to several days may be needed for the measurement of one polarization value only, for instance in the Cooper minimum of Hg6s.

By performing such measurements at different angles of emission θ an angular distribution of the spin polarization like that one shown in Fig. 13 for the Xe$^+$ $^2P_{1/2}$ final ionic state is obtained.[37] $A(\theta)$ is the spin polarization component parallel to the photon spin. A least-squares fit through the experimental values yields two spin parameters A and α and the β parameter describing the differential cross section. Knowledge of the wavelength dependence of these parameters yields information on the photoionization dynamics.
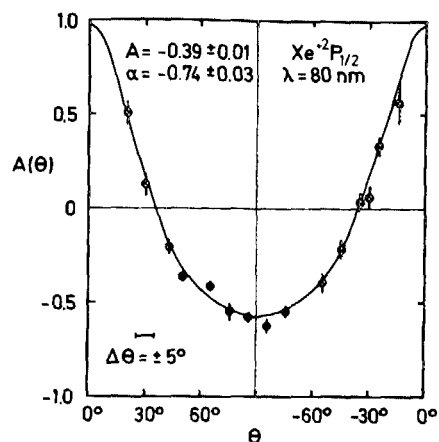

FIG. 13. Angular distribution of the spin-polarization component $A(\theta)$ obtained with circularly polarized radiation at 80 nm for Xe$^+$ $^2P_{1/2}$ final ionic state.[37,39] The full curve is a least-squares fit through the experimental points yielding the spin parameters A and α.

Thus a complete quantum mechanical characterization of the process considered could be performed.[42]

At the exit slit 2 two complementary methods for electron spin polarization analysis have been used for photoemission studies on nonmagnetic solids and adsorbates: a Mott detector and a LEED detector. Spin polarization measurements on a Pt(111) single crystal in normal[43–46] and off-normal emission[47,48] revealed pronounced structures which are often only weak in intensity spectra. These data of photoemission from nonmagnetic crystals with subsequent electron spin polarization analysis provided a quantitative characterization of the symmetry properties of electron bands. Thus a spin-resolved band mapping could be performed for Pt(111). In accordance with the spin polarization data for free atoms (Fig. 13, $\theta = 0°$), an almost complete polarization of electrons in normal emission has been observed, if the photoemission is studied at very low temperatures of the crystal (30 K).[46] Figure 14 shows an example obtained with the LEED detector.[47] The polarization distribution measured at a high-point density over the whole spectrum demonstrates the feasibility of experimental symmetry analysis of energy bands even near critical points in Pt.
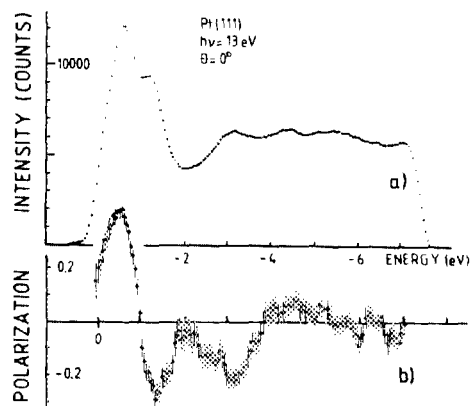

FIG. 14. Intensity distribution and corresponding spin polarization of photoelectrons of Pt(111) as a function of binding energy measured with the LEED spin detector. The spectrum was recorded in normal incidence and normal emission at a photon energy of $h\nu = 13$ eV.[45]
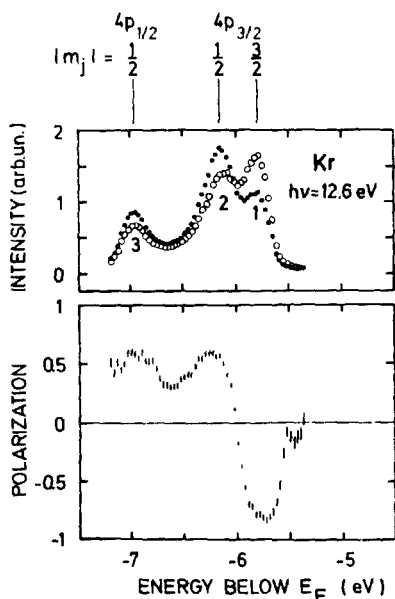
FIG. 15. Spin-resolved photoelectron spectra of a Kr monolayer on a Pt(111) substrate.[49] Upper part: photoelectron intensities in the counters of the Mott detector. Lower part: corresponding spin polarization in the direction of the light helicity. The assignments of the j and m_j state quantum numbers given follow from the sign of the spin polarization measured.

In order to pursue the behavior of the electronic structure in going from a free atom to a crystal structure the electron polarization of physisorbed rare gas atoms on a clean Pt surface was investigated. As an example Fig. 15 shows a photoelectron spectrum of physisorbed Kr (upper part) recorded with the two Mott-detector channels.[49] The fine structure splitting is nearly equal to the atomic case but the $p_{3/2}$ state is split into two peaks due to the lateral interactions in the adlayer. The sign of the spin polarization of the three peaks determines unequivocally the quantum numbers of the configuration and thus the order of the m_j values which has been a subject of controversy in the last years.

V. DISCUSSION

We have described the design and performance of the 6.5-m BESSY normal incidence monochromator of the Monk–Gillieson type which with up to 800-mA stored beam in the BESSY ring delivers photon fluxes of more than 10^{11} s^{-1} bandwidth^{-1} with a high degree of circular polarization. Even with the large angle optics and a virtual entrance slit, a source size limited resolution of 0.18 nm is obtained. The polarization of the radiation is in complete accordance with calculations based on Schwinger's theory, indicating that depolarization is negligible.

During three years of operation the monochromator has proved to be a reliable source of monochromatized and circularly polarized VUV radiation which has enabled low-signal experiments with a high sophistication to be performed. Some examples in the field of photoemission from atoms, adsorbates, and solids have been given.

ACKNOWLEDGMENTS

[1] Synchrotron Radiation: Techniques and Applications, edited by C. Kunz (Springer, Berlin, 1979).
[2] Synchrotron Radiation Research, edited by H. Winick and S. Doniach (Plenum, New York, 1980).
[3] Handbook on Synchrotron Radiation, edited by E.-E. Koch (North Holland, Amsterdam, 1983), Vols. 1a and 1b.
[4] Proceedings of the National and International Conferences on Synchrotron Radiation Instrumentation, Nucl. Instrum. Methods 152, 172, 195, 208, 222.
[5] Reflecting Optics for Synchrotron Radiation, edited by M. R. Howells, SPIE Proc. 315 (1981).
[6] High Resolution Soft X-ray Optics, edited by E. Spiller, SPIE Proc. 316 (1981).
[7] U. Heinzmann, B. Osterheld, and F. Schäfers, Nucl. Instrum. Methods 195, 395 (1982).
[8] U. Heinzmann, J. Phys. B 13, 4353 (1980).
[9] A. Eyers, Ch. Heckenkamp, F. Schäfers, G. Schönhense, and U. Heinzmann, Nucl. Instrum. Methods 208, 303 (1983).
[10] D. L. Ederer, B. E. Cole, and J. B. West, Nucl. Instrum. Methods 172, 185 (1980).
[11] P. Gürtler, E. Roick, G. Zimmerer, and M. Pouey, Nucl. Instrum. Methods 208, 835 (1983).
[12] H. Wilcke, W. Böhmer, R. Hänsel, and N. Schwentner, Nucl. Instrum. Methods 208, 59 (1983).
[13] V. Saile, and J. B. West, Nucl. Instrum. Methods 208, 199 (1983).
[14] A. A. Sokolov and I. M. Ternov, Sov. Phys. JETP 4, 396 (1957).
[15] K. C. Westfold, Astrophys. J. 130, 241 (1959).
[16] P. Joos, Phys. Rev. Lett. 4, 558 (1960).
[17] V. Saile, Nucl. Instrum. Methods 152, 59 (1978).
[18] D. L. Ederer, Nucl. Instrum. Methods 195, 191 (1982).
[19] R. L. Johnson in Ref. 3, Chap. 3, p. 220.
[20] M. R. Howells, Nucl. Instrum. Methods 195, 215 (1982).
[21] G. S. Monk, J. Opt. Soc. Am. 17, 358 (1928).
[22] A. H. C. P. Gillieson, J. Sci. Instrum. 26, 335 (1949).
[23] J. T. Hall, Appl. Opt. 5, 1051 (1966).
[24] D. J. Schroeder, Appl. Opt. 5, 545 (1966).
[25] D. J. Schroeder, J. Opt. Soc. Am. 60, 1022 (1970).
[26] M. V. R. K. Murty, J. Opt. Soc. Am. 52, 768 (1962).
[27] H. T. Smyth, J. Opt. Soc. Am. 25, 312 (1935).
[28] H. Yoshinaga, B. Okazaki, and S. Tatsuoka, J. Opt. Soc. Am. 50, 437 (1960).
[29] G. R. Rosendahl, J. Opt. Soc. Am. 51, 1 (1961).
[30] J. A. R. Samson, Techniques of Vacuum Ultraviolet Spectroscopy (Wiley, New York, 1967).
[31] H. G. Beutler, J. Opt. Soc. Am. 35, 311 (1945).
[32] T. Namioka, J. Opt. Soc. Am. 49, 446, 460 (1959).
[33] G. Mülhaupt, in X-Ray Microscopy, edited by G. Schmahl and D. Rudolph (Springer, Berlin, 1984), p. 4.
[34] W. Peatman, Nucl. Instrum. Methods 222, 6 (1984).
[35] W. R. Hunter, Appl. Opt. 17, 1259 (1978).
[36] F. P. Wolf, Technischer Bericht BESSY TB67, 1985.
[37] Ch. Heckenkamp, F. Schäfers, G. Schönhense, and U. Heinzmann, Phys. Rev. Lett. 52, 421 (1984).
[38] J. Schwinger, Phys. Rev. 75, 1912 (1949).
[39] Ch. Heckenkamp, Ph.D. thesis, Freie Universität Berlin, 1984.
[40] J. A. R. Samson, Nucl. Instrum. Methods 152, 225 (1978).
[41] J. T. Cox, G. Hass, J. B. Ransey, and W. R. Hunter, J. Opt. Soc. Am. 63, 435 (1973).
[42] Ch. Heckenkamp, F. Schäfers, G. Schönhense, and U. Heinzmann, Phys. Rev. A 32, 1252 (1985).
[43] A. Eyers, Ph.D. thesis, Freie Universität Berlin, 1984.
[44] A. Eyers, F. Schäfers, G. Schönhense, U. Heinzmann, H. P. Oepen, K. Hünlich, J. Kirschner, and G. Borstel, Phys. Rev. Lett. 52, 1559 (1984).
[45] H. P. Oepen, K. Hünlich, J. Kirschner, A. Eyers, F. Schäfers, G. Schönhense, and U. Heinzmann, Phys. Rev. B 31, 6846 (1985).
[46] A. Eyers, G. Schönhense, U. Friess, F. Schäfers, and U. Heinzmann, Surf. Sci. 162, 96 (1985).
[47] H. P. Oepen, Ph.D. thesis, Technische Universität Aachen, 1984; and Jül-Bericht 1970, 1985.
[48] H. P. Oepen, K. Hünlich, and J. Kirschner, Phys. Rev. Lett. 56, 496 (1986).
[49] G. Schönhense, A. Eyers, U. Friess, F. Schäfers, and U. Heinzmann, Phys. Rev. Lett. 54, 547 (1985).